# Measurement of the Isolated Prompt Photon Cross Section in $\bar{p}p$ Collisions at $\sqrt{s} = 1.8$ TeV

F. Abe,[9] D. Amidei,[4] G. Apollinari,[16] M. Atac,[4] P. Auchincloss,[15] A. R. Baden,[6] N. Bacchetta,[11] M. W. Bailey,[14] A. Bamberger,[4],[a] P. de Barbaro,[15] B. A. Barnett,[8] A. Barbaro-Galtieri,[10] V. E. Barnes,[14] T. Baumann,[6] F. Bedeschi,[13] S. Behrends,[2] S. Belforte,[13] G. Bellettini,[13] J. Bellinger,[21] D. Benjamin,[20] J. Bensinger,[2] A. Beretvas,[4] J. P. Berge,[4] S. Bertolucci,[5] S. Bhadra,[7] M. Binkley,[4] D. Bisello,[11] R. Blair,[1] C. Blocker,[2] A. Bodek,[15] V. Bolognesi,[13] A. W. Booth,[4] C. Boswell,[8] G. Brandenburg,[6] D. Brown,[6] E. Buckley-Geer,[17] H. S. Budd,[15] G. Busetto,[11] A. Byon-Wagner,[4] K. L. Byrum,[21] C. Campagnari,[3] M. Campbell,[3] A. Caner,[4] R. Carey,[6] W. Carithers,[10] D. Carlsmith,[21] J. T. Carroll,[4] R. Cashmore,[4],[a] A. Castro,[11] F. Cervelli,[13] K. Chadwick,[4] G. Chiarelli,[5] W. Chinowsky,[10] S. Cihangir,[4] A. G. Clark,[4] M. Cobal,[13] D. Connor,[12] M. Contreras,[3] J. Cooper,[4] M. Cordelli,[5] D. Crane,[4] M. Curatolo,[5] C. Day,[4] F. DeJongh,[4] S. Dell'Agnello,[13] M. Dell'Orso,[13] L. Demortier,[2] B. Denby,[4] P. F. Derwent,[3] T. Devlin,[17] D. DiBitonto,[18] M. Dickson,[15] R. B. Drucker,[10] K. Einsweiler,[10] J. E. Elias,[4] R. Ely,[10] S. Eno,[3] S. Errede,[7] B. Esposito,[5] A. Etchegoyen,[4],[a] B. Flaugher,[4] G. W. Foster,[4] M. Franklin,[6] J. Freeman,[4] H. Frisch,[3] T. Fuess,[4] Y. Fukui,[9] A. F. Garfinkel,[14] A. Gauthier,[7] S. Geer,[4] D. W. Gerdes,[3] P. Giannetti,[13] N. Giokaris,[16] P. Giromini,[5] L. Gladney,[12] M. Gold,[10] K. Goulianos,[16] H. Grassmann,[11] J. Grieco,[13] C. Grosso-Pilcher,[3] C. Haber,[10] S. R. Hahn,[4] R. Handler,[21] K. Hara,[19] B. Harral,[12] R. M. Harris,[4] J. Hauser,[4] C. Hawk,[17] T. Hessing,[18] R. Hollebeek,[12] L. Holloway,[7] P. Hu,[17] B. Hubbard,[10] B. T. Huffman,[14] R. Hughes,[12] P. Hurst,[5] J. Huth,[4] J. Hylen,[4] M. Incagli,[13] T. Ino,[19] H. Iso,[19] H. Jensen,[4] C. P. Jessop,[6] R. P. Johnson,[4] U. Joshi,[4] R. W. Kadel,[10] T. Kamon,[18] S. Kanda,[19] D. A. Kardelis,[7] I. Karliner,[7] E. Kearns,[6] L. Keeble,[18] R. Kephart,[4] P. Kesten,[2] R. M. Keup,[7] H. Keutelian,[4] D. Kim,[4] S. Kim,[19] L. Kirsch,[2] K. Kondo,[19] J. Konigsberg,[6] E. Kovacs,[4] S. E. Kuhlmann,[1] E. Kuns,[17] A. T. Laasanen,[14] J. I. Lamoureux,[21] S. Leone,[13] J. Lewis,[4] W. Li,[1] P. Limon,[4] T. M. Liss,[7] N. Lockyer,[12] M. Loreti,[11] E. Low,[12] C. B. Luchini,[7] P. Lukens,[4] P. Maas,[21] K. Maeshima,[4] M. Mangano,[13] J. P. Marriner,[4] M. Mariotti,[13] R. Markeloff,[21] L. A. Markosky,[21] R. Mattingly,[2] P. McIntyre,[18] A. Menzione,[13] T. Meyer,[18] S. Mikamo,[9] M. Miller,[3] T. Mimashi,[19] S. Miscetti,[5] M. Mishina,[9] S. Miyashita,[19] Y. Morita,[19] S. Moulding,[2] J. Mueller,[17] A. Mukherjee,[4] L. F. Nakae,[2] I. Nakano,[19] C. Nelson,[4] C. Newman-Holmes,[4] J. S. T. Ng,[6] M. Ninomiya,[19] L. Nodulman,[1] S. Ogawa,[19] R. Paoletti,[13] V. Papadimitriou,[4] A. Para,[4] E. Pare,[6] S. Park,[4] J. Patrick,[4] G. Pauletta,[13] L. Pescara,[11] T. J. Phillips,[6] F. Ptohos,[6] R. Plunkett,[4] L. Pondrom,[21] J. Proudfoot,[1] G. Punzi,[13] D. Quarrie,[4] K. Ragan,[12] G. Redlinger,[3] J. Rhoades,[21] M. Roach,[20] F. Rimondi,[4],[a] L. Ristori,[13] T. Rodrigo,[4] T. Rohaly,[12] A. Roodman,[3] W. K. Sakumoto,[15] A. Sansoni,[5] R. D. Sard,[7] A. Savoy-Navarro,[4] V. Scarpine,[7] P. Schlabach,[6] E. E. Schmidt,[4] O. Schneider,[10] M. H. Schub,[14] R. Schwitters,[6] A. Scribano,[13] S. Segler,[4] Y. Seiya,[19] M. Shapiro,[10] N. M. Shaw,[14] M. Sheaff,[21] M. Shochet,[3] J. Siegrist,[10] P. Sinervo,[12] J. Skarha,[8] K. Sliwa,[20] D. A. Smith,[13] F. D. Snider,[8] L. Song,[12] M. Spahn,[10] P. Sphicas,[4] R. St. Denis,[6] A. Stefanini,[13] G. Sullivan,[3] R. L. Swartz, Jr.,[7] M. Takano,[19] F. Tartarelli,[13] K. Takikawa,[19] S. Tarem,[2] D. Theriot,[4] M. Timko,[18] P. Tipton,[4] S. Tkaczyk,[4] A. Tollestrup,[4] J. Tonnison,[14] W. Trischuk,[6] N. Turini,[13] Y. Tsay,[3] F. Ukegawa,[19] D. Underwood,[1] S. Vejcik, III,[8] R. Vidal,[4] R. G. Wagner,[1] R. L. Wagner,[4] N. Wainer,[4] J. Walsh,[12] T. Watts,[17] R. Webb,[18] C. Wendt,[21] H. Wenzel,[13] W. C. Wester, III,[10] T. Westhusing,[13] S. N. White,[16] A. B. Wicklund,[1] H. H. Williams,[12] B. L. Winer,[15] J. Wyss,[11] A. Yagil,[4] K. Yasuoka,[19] G. P. Yeh,[4] J. Yoh,[4] M. Yokoyama,[19] J. C. Yun,[4] A. Zanetti,[13] F. Zetti,[13] and S. Zucchelli[4],[a]

(CDF Collaboration)

[1]*Argonne National Laboratory, Argonne, Illinois 60439*
[2]*Brandeis University, Waltham, Massachusetts 02254*
[3]*University of Chicago, Chicago, Illinois 60637*
[4]*Fermi National Accelerator Laboratory, Batavia, Illinois 60510*
[5]*Laboratori Nazionali di Frascati, Istituto Nazionale di Fisica Nucleare, Frascati, Italy*

[6]Harvard University, Cambridge, Massachusetts 02138
[7]University of Illinois, Urbana, Illinois 61801
[8]The Johns Hopkins University, Baltimore, Maryland 21218
[9]National Laboratory for High Energy Physics (KEK), Tsukuba, Ibaraki, Japan
[10]Lawrence Berkeley Laboratory, Berkeley, California 94720
[11]Università di Padova, Istituto Nazionale di Fisica Nucleare, Sezione di Padova, I-35131 Padova, Italy
[12]University of Pennsylvania, Philadelphia, Pennsylvania 19104
[13]Istituto Nazionale di Fisica Nucleare, University and Scuola Normale Superiore of Pisa, I-56100 Pisa, Italy
[14]Purdue University, West Lafayette, Indiana 47907
[15]University of Rochester, Rochester, New York 14627
[16]Rockefeller University, New York, New York 10021
[17]Rutgers University, Piscataway, New Jersey 08854
[18]Texas A&M University, College Station, Texas 77843
[19]University of Tsukuba, Tsukuba, Ibaraki 305, Japan
[20]Tufts University, Medford, Massachusetts 02155
[21]University of Wisconsin, Madison, Wisconsin 53706
(Received 4 February 1992)

We present a measurement of the cross section for production of isolated prompt photons in $\bar{p}p$ collisions at $\sqrt{s}=1.8$ TeV. The cross section, measured as a function of transverse momentum ($P_T$), agrees qualitatively with QCD calculations but has a steeper slope at low $P_T$.

PACS numbers: 13.85.Qk, 12.38.Qk

In this Letter we present the first measurement of the cross section for production of prompt photons in proton-antiproton collisions at $\sqrt{s}=1.8$ TeV. Prompt photons are produced in the initial collision, in contrast to photons produced by decays of hadrons. This measurement can be used to test quantum chromodynamics (QCD). In QCD, at lowest order, prompt photon production is dominated by the Compton process ($gq \rightarrow \gamma q$), which is sensitive to the gluon distribution of the proton. We measure prompt photons in a previously unexplored range of fractional momentum ($0.016 < x < 0.070$).

A detailed description of the Collider Detector at Fermilab (CDF) may be found in Ref. [1]; the components relevant for this analysis are described briefly here. We use a coordinate system with $z$ along the proton beam, azimuthal angle $\phi$, polar angle $\theta$, and pseudorapidity $\eta = -\ln\tan(\theta/2)$. Scintillator-based electromagnetic (EM) and hadronic (HAD) calorimeters in the central region ($|\eta| < 1.1$) are arranged in projective towers of size $\Delta\eta \times \Delta\phi \approx 0.1 \times 0.26$. The central electromagnetic strip chambers (CES) are multiwire proportional chambers embedded inside the central EM calorimeter near shower maximum (6 radiation lengths and 184 cm from the beam). The CES anode wires measure $\phi$ and cathode strips measure $\eta$; both views have a channel separation of roughly 8 mrad for measuring the transverse profile of electromagnetic showers. The central drift tubes (CDT) are three layers of gas counters just outside the central tracking chamber (CTC). In this analysis, the CDT measures electron-positron pairs from photons which convert in either the outer wall of the CTC or the inner two layers of the CDT (18% of a radiation length total).

Photon data were taken with a high threshold trigger and a prescaled low threshold trigger. An integrated luminosity of 3.3 (0.10) pb$^{-1}$ was acquired with the high (low) threshold trigger which required 23 (10) GeV of EM transverse energy; the triggers were 90% (98%) efficient for photons with 27 (14) GeV of $P_T$. Throughout this article $P_T$ is the component of the photon momentum transverse to the beam direction, and transverse energy is defined similarly. To reject jet backgrounds, these triggers required that at least 89% of the transverse energy of the photon be in the EM compartment of the calorimeter, and required the photon to be *isolated*: The extra transverse energy inside a cone of radius $R = [(\Delta\eta)^2 + (\Delta\phi)^2]^{1/2} = 0.7$ centered on the photon was required to be less than 2 GeV. The efficiency of this isolation cut, independent of photon $P_T$, was estimated to be 89.5%; this is the measured probability that an isolation cone in a minimum-bias event will contain less than 2 GeV.

A prompt photon candidate is an isolated cluster in the central EM calorimeter with no charged track pointing at the cluster. The only significant background sources are the decays of the neutral mesons $\pi^0$ and $\eta$ into photons. We employ two methods for statistically subtracting the neutral meson background from our photon candidates: The *profile method* uses the transverse profile of the electromagnetic shower in the CES and the *conversion method* counts electron-positron pairs from photon conversions which produce hits in the CDT.

For both methods, within the tower boundaries of a calorimeter energy cluster [2], we formed CES strip and wire clusters, each containing 11 channels (total width $\approx 0.1$ rad) centered on a seed channel with at least 0.5 GeV. The highest-energy strip cluster and the highest-energy wire cluster were chosen for measuring the transverse profile and position of the photon candidate. Backgrounds from $\eta$ mesons were reduced by requiring that any additional CES clusters within the boundaries of the

calorimeter energy cluster had less than 1 GeV each. The efficiency of this cut, ranging from 95% (at 14 GeV) to 81% (at 63 GeV), was determined from measurements of electrons in a test beam. Fiducial cuts were imposed to avoid uninstrumented regions at the edges of the CES; the region remaining was 66% of the solid angle for $|\eta| < 0.9$. To maintain the projective nature of the calorimeter tower, the $z$ position of the event vertex was required to be within 50 cm of the center of the detector; this cut was 88% efficient. Finally, cosmic-ray events which included bremsstrahlung photons had large transverse momentum imbalance which made them easy to identify and remove. The data sample for the conversion method came from the high threshold trigger, and the analysis used the same selection cuts with the following additional cuts to reduce backgrounds: CES average $\tilde{\chi}^2 < 8$ (defined below), azimuthal separation between CDT hits and the CES cluster $\Delta\phi < 0.07$, and $z$ separation between CDT hits and the CES cluster $\Delta z < 10$ cm (at 1.4 m from the beam). The total acceptance $\alpha$, including efficiency, for the profile (conversion) method was between 50% (44%) and 43% (40%) depending on $P_T$.

The transverse profile of each photon candidate was compared to that measured for electrons in a test beam. A measure of the goodness of fit ($\tilde{\chi}^2$ [3]) was usually larger for a neutral meson (poor fit) than for a single photon (good fit) because a neutral meson usually produced a wider EM shower. The $\tilde{\chi}^2$ variable is arbitrarily normalized and has a mean value of approximately 2.5 for electron showers. The *average* of $\tilde{\chi}^2$ in both views [(strip $\tilde{\chi}^2$+wire $\tilde{\chi}^2$)/2] was the variable used to separate single photons from neutral mesons in the profile method.

After all cuts, the final sample was roughly half signal and half background. The number of photons ($N_\gamma$) in a bin of $P_T$ is obtained in each method from the number of photon candidates ($N$), the method's efficiency for photon candidates ($\epsilon$), and the corresponding efficiency for true photons ($\epsilon_\gamma$) and background ($\epsilon_b$), using

$$N_\gamma = \left(\frac{\epsilon - \epsilon_b}{\epsilon_\gamma - \epsilon_b}\right) N . \quad (1)$$

Equation (1) comes from $\epsilon N = \epsilon_\gamma N_\gamma + \epsilon_b N_b$ with $N_b = N - N_\gamma$. For the profile method, the efficiency $\epsilon$ is the fraction of events which have $\tilde{\chi}^2 < 4$ out of all events with $\tilde{\chi}^2 < 20$. For the conversion method, $\epsilon$ is the fraction of photon candidates which produce a conversion hit in the CDT.

For the profile method we estimated $\epsilon_\gamma$ and $\epsilon_b$ using a detector simulation. The simulation employed real electron showers, measured in a test beam, and corrected for differences between photons and electrons. Figure 1 shows that we obtain good agreement between the data and simulation for the strip $\tilde{\chi}^2$ distribution of single photons from $\eta$-meson decays, and for the average $\tilde{\chi}^2$ distribution of single $\pi^0$'s from $\rho$-meson decays. There were

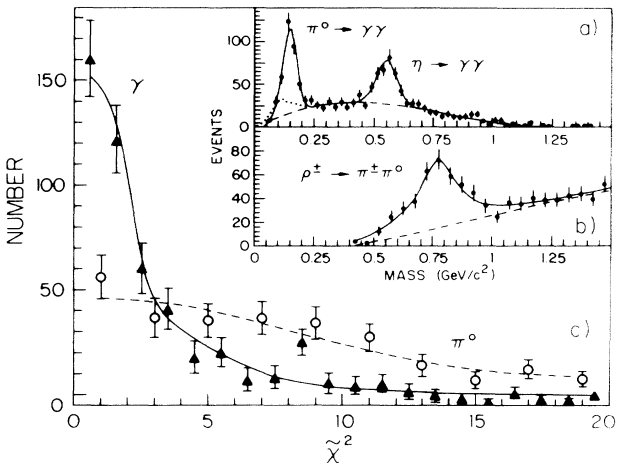


FIG. 1. (a) The invariant mass of two photons from meson decays (points), a two-Gaussian plus background fit (solid curve), the polynomial-like background (dashed curve), and the expected background from misidentified single photons (dotted curve). (b) The invariant mass of a neutral cluster and charged track (points) compared to a Breit-Wigner plus background fit (solid curve) and a polynomial background (dashed curve). (c) The $\tilde{\chi}^2$ distributions of photons (triangles) from $\eta$ decays in (a) and of $\pi^0$'s (circles) from $\rho$ decays in (b) compared to a detector simulation (curves).

three sources of systematic uncertainty in the simulation of the photon efficiency $\epsilon_\gamma$: the transverse shape of photon-induced electromagnetic showers, the statistical fluctuations in the transverse profile of photons, and the linearity of gas gain response of the CES to electrons in the electromagnetic shower. Figure 2(a) shows the measured efficiency $\epsilon$ for the profile method, as a function of transverse momentum, along with the simulated efficiencies $\epsilon_\gamma$ and $\epsilon_b$ and their total systematic bounds. To obtain $\epsilon_b$ we simulated the neutral mesons $\pi^0$, $\eta$, and $K_S^0$ with a relative production ratio of 1:1:0.4 determined as follows. From the data shown in Fig. 1(a), using three-channel CES clusters, we measured the ratio of *isolated* $\eta$ to $\pi^0$ production at 12 GeV: $\eta/\pi^0 = 1.02 \pm 0.15(\text{stat}) \pm 0.23(\text{syst})$ [3]. The ratio $K_S^0/\pi^0 \approx 0.4$ for $P_T > 3$ GeV is implied from our previously reported measurement of $K_S^0/\pi^+$ and isospin invariance [4]. The systematic uncertainty induced by the uncertainties in these measurements has been included in the systematic bound on the background efficiency; however, the background systematic uncertainty is dominated by the three previously mentioned uncertainties in the photon efficiency. Figure 2(b) shows that the simulated $\tilde{\chi}^2$ distribution of photons and background, combined in the relative proportions predicted by the profile method, is in good agreement with the data. At high $P_T$ the two photons from the decay of a $\pi^0$ are so close together that the $\tilde{\chi}^2$ efficiency for the background is almost the same as for a single photon; consequently, the profile method was only used up to $P_T = 40$ GeV/$c$.

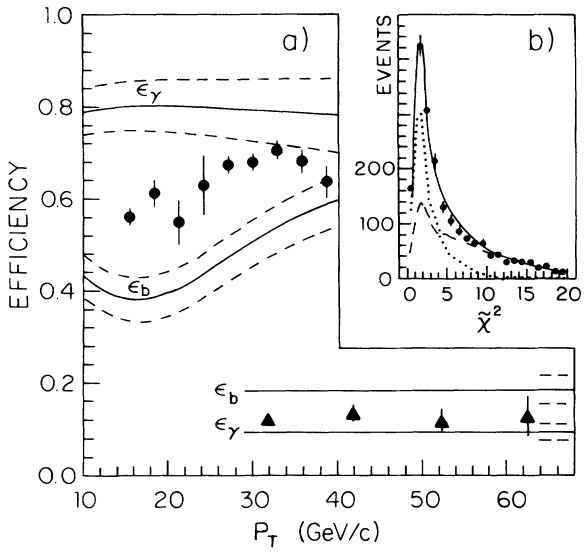


FIG. 2. (a) The efficiency of photon candidates (points), and simulated photons and background (solid curves) with systematic bounds (dashed curves) for the profile method (circles) and for the conversion method (triangles). The bounds on $\epsilon_\gamma$ and $\epsilon_b$ are completely correlated within each method. (b) The $\tilde{\chi}^2$ distribution of data (points) with $P_T < 27$ GeV/$c$ compared to our simulation of photons (dotted curve), background (dashed curve), and their sum (solid curve).

For the conversion method, we estimate the production ratio $\gamma/\pi^0$ at low $P_T$ from the azimuthal separation of the CDT hit and the highest-energy CES cluster. From this ratio, the number of prompt photon candidates, and the total number of CDT hits associated with the prompt photon candidates, we estimated the efficiency of photon conversion and detection to be $0.095 \pm 0.014(\text{stat}) \pm 0.010(\text{syst})$. The efficiency expected from the amount of material and the selection cuts is about 11%, consistent with this estimate. The uncertainty in the efficiency, which is independent of $P_T$, dominated the uncertainty in the normalization of the cross section from the conversion method. The efficiency of conversion and detection for the background is estimated from the photon efficiency and a simulation of the background from $\pi^0$, $\eta$, and $K_S^0$ mesons. The background efficiency is the same, within errors, as the naive probability of observing at least one photon conversion from a two-photon decay: $\epsilon_b = 2\epsilon_\gamma - \epsilon_\gamma^2$. Figure 2(a) shows the measured conversion efficiency $\epsilon$, for the conversion method, as a function of transverse momentum, along with the estimated efficiencies $\epsilon_\gamma$ and $\epsilon_b$ and their total systematic bounds.

From the number of prompt photons ($N_\gamma$) in a bin of transverse momentum ($\Delta P_T$) and a range of pseudorapidity ($\Delta\eta = 1.8$), using the acceptance ($a$) and the integrated luminosity ($\mathcal{L}$), we obtain the isolated prompt photon cross section:

$$\frac{d^2\sigma}{dP_T\,d\eta} = \frac{N_\gamma}{\Delta P_T \Delta\eta\, a\mathcal{L}}, \qquad (2)$$

TABLE I. The cross section for isolated prompt photons, the statistical uncertainty, and the $P_T$-dependent component of the systematic uncertainty. There is an additional normalization systematic uncertainty of 27% in common among the first eleven entries (profile method), and $^{+32}_{-46}$% for the last four entries (conversion method).

| $P_T$ bin (GeV/$c$) | $P_T$ (GeV/$c$) | $d^2\sigma/dP_T\,d\eta$ [pb/(GeV/$c$)] | Stat. (%) | Syst. (%) |
|---|---|---|---|---|
| 14–15 | 14.5 | $3.16\times10^3$ | 11 | 21 |
| 15–17 | 15.9 | $1.55\times10^3$ | 12 | 13 |
| 17–19 | 17.9 | $1.03\times10^3$ | 13 | 6 |
| 19–22 | 20.4 | $4.36\times10^2$ | 18 | 2 |
| 22–27 | 24.2 | $1.91\times10^2$ | 22 | 12 |
| 27–28 | 27.5 | $1.30\times10^2$ | 12 | 23 |
| 28–29 | 28.5 | $1.13\times10^2$ | 12 | 26 |
| 29–31 | 30.0 | $7.15\times10^1$ | 12 | 32 |
| 31–33 | 32.0 | $6.98\times10^1$ | 11 | 40 |
| 33–35 | 34.0 | $3.78\times10^1$ | 20 | 50 |
| 35–40 | 37.3 | $2.23\times10^1$ | 20 | 71 |
| 28–38 | 32.2 | $6.05\times10^1$ | 15 | 7 |
| 38–48 | 42.4 | $1.19\times10^1$ | 37 | 6 |
| 48–58 | 52.5 | $6.53\times10^0$ | 41 | 6 |
| 58–68 | 62.6 | $2.22\times10^0$ | 79 | 8 |

which is shown in Fig. 3 and tabulated in Table I. Here we present the profile method in the low-$P_T$ region ($14 < P_T < 40$ GeV/$c$) and the conversion method in the high-$P_T$ region ($28 < P_T < 68$ GeV/$c$). The two methods

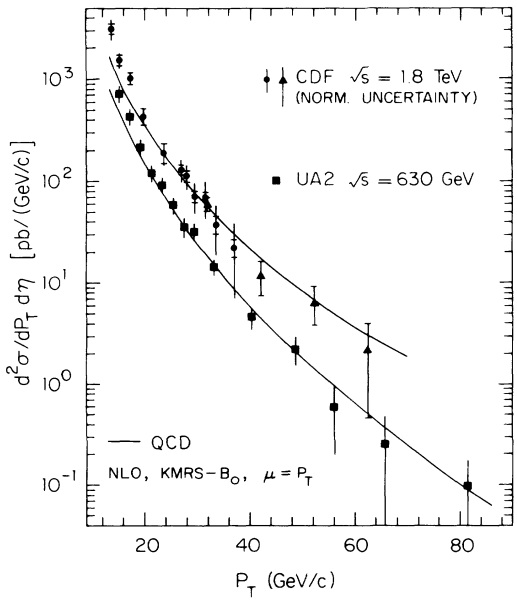


FIG. 3. The isolated prompt photon cross section, from both CDF (circles and triangles) and UA2 [7] (squares), compared to recent QCD predictions (curves). The profile method (circles) and conversion method (triangles) have separate normalization uncertainties shown in the legend. The next-to-leading order (NLO) predictions [5] use current parton distributions (KMRS-$B_0$ [6]) and a standard renormalization scale ($\mu = P_T$).

agree in the region in which they overlap. In Fig. 3, the inner error bars are the statistical uncertainty and the outer error bars are the $P_T$-dependent part of the systematic uncertainty combined in quadrature with the statistical uncertainty. The $P_T$-independent component of the systematic uncertainty is shown as the normalization uncertainty separately for each of the two methods.

In Fig. 3 our measurements are compared to a next-to-leading order QCD calculation [5] using a single set of parton distributions [6] at a renormalization scale $\mu = P_T$. The QCD prediction changes by less than 30% when the parton distributions are varied among commonly used sets; it decreases (increases) by 12% when the renormalization scale is double (halved). The calculation includes the experimental isolation cut. Figure 3 shows that the measured cross section agrees qualitatively with QCD calculations but has a steeper slope at low $P_T$. Data acquired at the CERN $\bar{p}p$ collider [7] ($\sqrt{s} = 630$ GeV) show similar behavior. One possible cause of the difference between the data and the QCD calculation is the bremsstrahlung process [8,9], prevalent at low $P_T$, in which a final-state quark radiates a photon.

We thank the Fermilab staff and the technical staffs of the participating institutions for their vital contributions. This work was supported by the U.S. Department of Energy and National Science Foundation, the Italian Istituto Nazionale di Fisica Nucleare, the Ministry of Science, Culture and Education of Japan, and the Alfred P. Sloan Foundation. We also wish to thank J. F. Owens for providing his computer code for the theoretical calculations.

---

[a] Visitor.

[1] F. Abe *et al.*, Nucl. Instrum. Methods Phys. Res., Sect. A **271**, 387 (1988).
[2] F. Abe *et al.*, Phys. Rev. D **43**, 2070 (1991).
[3] F. Abe *et al.*, Fermilab Report No. Fermilab-PUB-92/01-E, 1992 (to be published).
[4] M. Schub, Ph.D. thesis, Purdue University, 1989.
[5] H. Baer, J. Ohnemus, and J. F. Owens, Phys. Lett. B **234**, 127 (1990).
[6] See $B_0$ in J. Kwiecinski, A. D. Martin, R. G. Roberts, and W. J. Stirling, Phys. Rev. D **42**, 3645 (1990).
[7] UA2 Collaboration, J. Alitti *et al.*, Phys. Lett. B **263**, 544 (1991).
[8] E. Pilon, P. Aurenche, M. Fontannaz, and J. Guillet, in Proceedings of the XXVI Recontre de Moriond, Les Arcs, France, 1991 (to be published).
[9] E. Berger and J. Qiu, Phys. Rev. D **44**, 2002 (1991).